THE JOURNAL OF PHYSICAL CHEMISTRY Letters

Letter

Cite This: J. Phys. Chem. Lett. 2019, 10, 2008−2016

pubs.acs.org/JPCL

# Low-Dimensional Confined Ice Has the Electronic Signature of Liquid Water

Yonghwan Yun,[†] Rustam Z. Khaliullin,*[,§] and Yousung Jung*[,†,‡]

[†]Department of Chemical and Biomolecular Engineering and [‡]Graduate School of Energy Environment Water and Sustainability (EEWS), Korea Advanced Institute of Science and Technology (KAIST), 291 Daehakro, Daejeon 305-701, Korea

[§]Department of Chemistry, McGill University, 801 Sherbrooke Street West, Montreal, QC H3A 0B8, Canada

Supporting Information

**ABSTRACT:** Water confined in nanomaterials demonstrates anomalous behavior. Recent experiments and simulations have established that room-temperature water inside carbon nanotubes and between graphene layers behaves as solid ice: its molecules form four hydrogen bonds in a highly organized network with long-range order and exhibit low mobility. Here, we applied a first-principle energy decomposition analysis to reveal that the strength and patterns of donor−acceptor interactions between molecules in these low-dimensional ice structures resemble those in bulk liquid water rather than those in hexagonal ice. A correlation analysis shows that this phenomenon originates from a variety of hydrogen-bond distortions, different in 1D and 2D ice, from the tetrahedral configuration due to constraints imposed by nanomaterials. We discuss the implications of the reported interplay between the electronic and geometric structure of hydrogen bonds in "room-temperature ice" for computer modeling of confined water using traditional force fields.

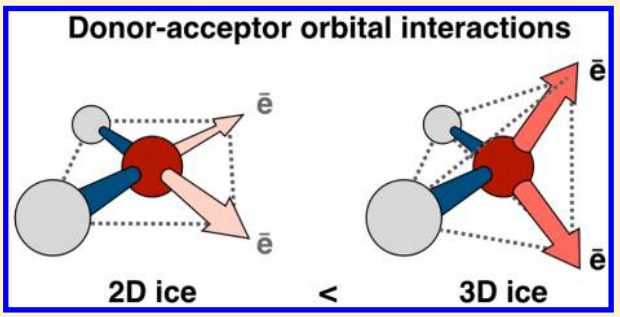




Understanding the behavior of water under confinement is crucial for various applications in energy and water treatment[1−5] as well as for studying intrinsic properties of water itself.[6] When water is confined in low dimensions, its hydrogen bond (HB) network behaves differently from that of its bulk counterpart, resulting in unusual structure, dynamics, and phase behavior.[7−24] For instance, even at room temperature, confined water crystallizes into unique solid phases that are not observed in the phases diagram of bulk ice.[8,9,19−24]

Carbon nanotubes (CNTs) and graphene provide well-defined low-dimensional environments to study water confinement effects in a systematic way. CNTs have a one-dimensional (1D) channel with a diameter between 1.1 and 1.4 nm where water molecules form a stack of ordered polygonal ring structures called "ice nanotubes."[8,9] Each water molecule in the ice nanotube coordinates with approximately four neighboring molecules, and is highly immobile with the self-diffusion coefficient reported to be several orders of magnitude lower than that of bulk liquid water.[8,10,24] Raman spectroscopy measurements have demonstrated recently that these ice nanotubes have elevated freezing temperatures as high as 411 K for a 1.05 nm CNT.[25]

At the same time, graphene layers provide ideal two-dimensional (2D) channels. Recent transmission electron microscopy (TEM) measurements showed that a monolayer of "square ice" with a lattice constant approximately 2.83 Å is formed in graphene nanocapillaries at room temperature,[22] although the latter interpretation of exact square symmetry might have been caused by sodium chloride contamination.[26] Numerous molecular dynamics (MD) studies using classical force fields have reported a monolayer of "square ice" in hydrophobic nanocapillaries.[18,22−24,27,28] More recently, *ab initio* studies also found that the planar square ice forms under 2D confinement.[29−31] Therefore, theoretical and computational investigations commonly predict "square ice" in agreement with the experiment although the precise conditions (usually pressure) under which "square ice" is formed are sensitive to the details of a computational setup.

We note that the empirical force-fields employing point charge models and Lennard-Jones potential are parametrized to reproduce the bulk properties and neglect the charge transfer (CT) interactions between molecules. However, at the most fundamental level of water modeling, it has been recognized that a typical HB involves the quantum mechanical CT from the electron-donor molecule to the virtual orbitals of electron-acceptor molecule.[32−43] Although the quantitative contribution of the CT effect to the overall binding energy is computed differently in various theoretical approaches it is clear that, even with conservative estimates, donor−acceptor orbital interactions between molecules play an important role in physics and chemistry of bulk water.[44] Multiple studies[45−51] have pointed out a connection between the donor−acceptor interactions and measurable properties of bulk liquid water

Received: April 1, 2019
Accepted: April 4, 2019
Published: April 4, 2019




DOI: 10.1021/acs.jpclett.9b00921
J. Phys. Chem. Lett. 2019, 10, 2008−2016

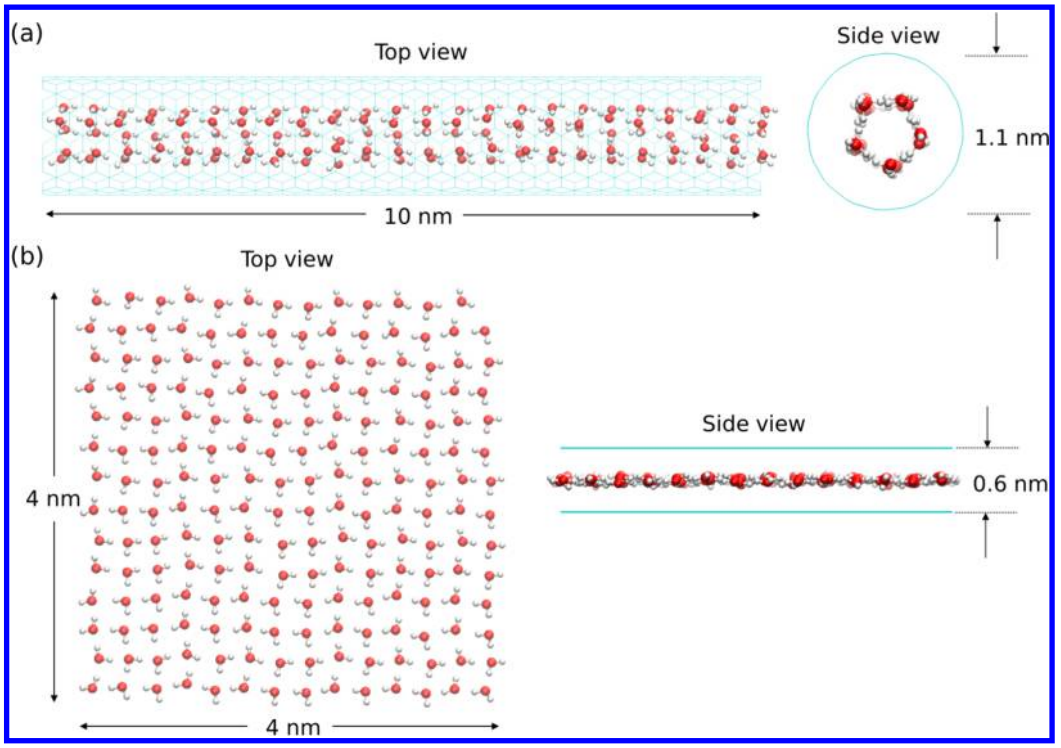


**Figure 1.** Snapshots of the top and side views of the systems studied in this work. Oxygen atom is in red, hydrogen in white, and carbon in green. (a) Water molecules inside (8, 8) CNT take a series of ordered pentagonal ring structures. (b) Water molecules confined between two graphene layers form a monolayer 2D ice.

such as features of the X-ray absorption, infrared, and nuclear magnetic resonance spectra. It is therefore essential to perform a comparative analysis of donor−acceptor electronic interactions in bulk water and in extreme low-dimensional environments.

In this work, we studied the 1D and 2D ice structures inside (8, 8) CNT and graphene as well as structures of bulk liquid water and hexagonal ice. We used the energy decomposition analysis (EDA) method based on absolutely localized molecular orbitals (ALMO)[38] to investigate the electronic structure of the HB network configurations obtained from classical molecular dynamics (MD) simulations. As mentioned above, the extent of donor−acceptor interactions in HB is defined and computed differently in the conventional EDA methods.[33,38,40,41,52−54] For example, natural bond orbital analysis[52] and natural energy decomposition analysis[33] suggest that charge transfer is the major component of HB because when charge transfer is neglected these methods yielded no binding at the water dimer equilibrium geometry. On the other hand, early EDA methods,[53,54] their modern variants[35,38,55] and symmetry-adapted perturbation theory[40,41] show that charge transfer contributes about ∼20−30% of the overall binding energy between water molecules in small clusters, in agreement with the long-held intuitive view of HBs. After a debate spanning several decades, it has been argued that the family of methods based on natural bond orbital analysis are not optimal for weak interactions.[43] It appears that the covalent component of HB is better described by the Kitaura−Morokuma family of EDA methods as well as by symmetry-adapted perturbation theory. It is important to emphasize, however, that the focus of this work is not on the absolute values of CT terms but on the comparative strength of the CT effect in bulk and low-dimensional phases of water, which is expected to be less sensitive to the choice of an EDA method. We utilized ALMO EDA in this work because it describes CT in agreement with a wide variety of EDA methods, because it is implemented for extended systems under periodic boundary conditions,[56] and, most importantly, because it has an ability to evaluate the strength of CT donor−acceptor orbital interactions in individual hydrogen bonds.[38]

Using the CT energy as a convenient descriptor of an individual HB, we compared HB networks in 1D and 2D ice, bulk hexagonal ice, and liquid water. Our comparative analysis reveals that the strength of the donor−acceptor HB interactions in 1D and 2D ice is not as high as in hexagonal ice and is rather close to that in bulk liquid water. Detailed structural analyses reveal that the distinct electronic interactions of the low-dimensional ice originate from the highly nontetrahedral geometry that is not seen in the phase diagram of bulk ice.

The (8, 8) CNT and two graphene sheets were used to model 1D and 2D confining channels, respectively. A description illustrating the model system is present in Figure 1. The diameter of CNT (1.1 nm) and the distance between two graphene layers (0.6 nm) were chosen to form the ice structures in low-dimensional materials that are observed experimentally. 1D ice and 2D ice in this work refer to the water confined in (8, 8) CNT and two graphene layers, respectively.

We employed two different levels of theory for our calculations. First, we implemented classical MD simulations of water with the extended simple point charge (SPC/E)[57] water model at room temperature to investigate the phase behaviors and obtain configurations of confined water. The use of classical force fields to obtain trajectories of water at



DOI: 10.1021/acs.jpclett.9b00921
J. Phys. Chem. Lett. 2019, 10, 2008−2016

different environments was motivated by the facts that our attempt to perform *ab initio* MD under ambient pressure failed to reproduce square-like planar water structure within graphene and that instead the force fields yielded the water structures under confinements consistent with experiments. Second, we performed ALMO EDA to quantify the strength of donor−acceptor interactions for each HBs. ALMO EDA decomposes the total intermolecular binding energy ($\Delta E_{TOT}$) into the frozen-density energy ($\Delta E_{FRZ}$), intramolecular polarization energy ($\Delta E_{POL}$), and charge-transfer energy ($\Delta E_{CT}$) and a generally small higher-order ($\Delta E_{HO}$) relaxation term (see Khaliullin et al.[38] for a detailed description of the ALMO EDA terms).

$$\Delta E_{TOT} = \Delta E_{FRZ} + \Delta E_{POL} + \Delta E_{CT} + \Delta E_{HO} \quad (1)$$

$$\Delta E_{CT} = \sum_{A,D=1}^{Mol} \Delta E_{D\rightarrow A} \quad (2)$$

Like all other EDA methods based on density functional theory, ALMO EDA does not provide a well-defined recipe to decompose the frozen-density and polarization terms into molecular contributions (e.g., single-molecule, two-body terms). While these terms contribute to the overall stabilization of the HB network, this work focuses on the CT energies that can be readily decomposed into pairwise contributions as shown in eq 2.[38] A two-body term $\Delta E_{D\rightarrow A}$ corresponds to the orbital relaxation arising from the charge transfer from the occupied orbitals of electron-donor molecule D to the virtual orbitals of electron-acceptor molecule A. This decomposition enables us to understand the nature of CT interactions in the HB network in a physically meaningful way: the two-body terms provide an accurate description of the strength of donor−acceptor interactions in individual HB moieties since they are obtained self-consistently and include HB cooperativity effects. Again, we note that the ALMO CT energies have been shown to be good predictors for experimentally measurable properties of bulk liquid water.

To examine the phase behavior of confined water, we first investigate the structural and dynamical properties of water from the MD trajectories. In the 1D confined system, we computed the axial oxygen−oxygen radial distribution function (RDF) $g_z(r)$ to characterize the molecular structure (Figure 2a). The $g_z(r)$ exhibits layers of ordered pentagonal ice nanotubes along the axis of CNT. We examined dynamical properties of the 1D water by computing the axial diffusion coefficient $D_z$ from the slope (taken as 1−2 ns) of the mean-square displacement (MSD) using Einstein's relation. The diffusion coefficient normalized to that of bulk liquid water $D_{1D,z}/D_{liquid,z} = 4.4 \times 10^{-6}$ indicates that the 1D confined water is highly immobilized. As in the case of the 1D system, we computed the lateral oxygen−oxygen RDF $g_{xy}(r)$ and diffusion coefficient $D_{xy}$ parallel to graphene in the 2D confined water. The $g_{xy}$(r) of the 2D confined water shows pronounced peaks and minima between them, characteristic of a solid over a long range (Figure 2b). The diffusion coefficient normalized to bulk liquid water $D_{2D,xy}/D_{liquid,xy} = 2.0 \times 10^{-4}$ indicates that the 2D confined water is much less fluid compared to bulk water. Therefore, the formation of solid ice under 1D and 2D confinement at room temperature is evident based on both the long-range order and low molecular mobility.

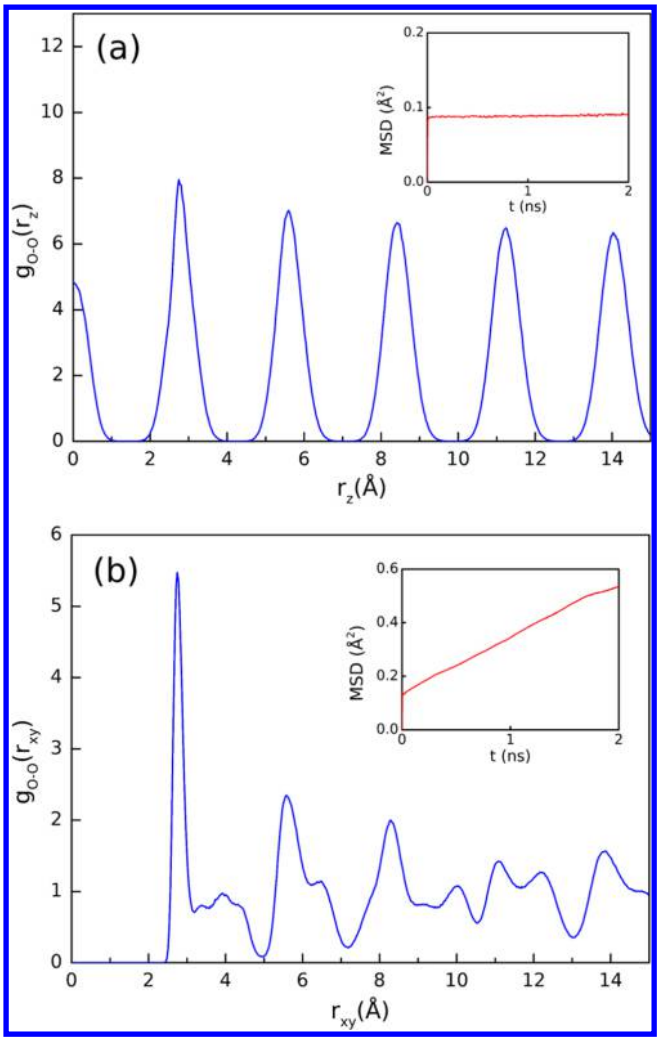


**Figure 2.** (a) Axial oxygen−oxygen radial distribution function and mean-square displacement (inset) for the 1D ice along the axis of CNT. (b) Lateral oxygen−oxygen radial distribution function and mean-square displacement (inset) for the 2D ice projected on the *xy* plane.

We calculated the average CT energy per water molecules to characterize the strength of donor−acceptor interactions in confined ice (Figure 3). The first two strongest CT energies, which account for approximately 90% of the total molecular CT energy, correspond to the interaction with two adjacent water molecules, and the sum of the remaining interactions corresponds to the "etc." The remaining "etc." term of low-dimensional water decreases to 3−5% compared to 8% of liquid water, which reflects the high degree of the ordered HB network with two donor and two acceptor bonds. The "BD" term in Figure 3 refers to the combined back-donation terms, that is, back-donation from a typical electron-acceptor molecule to a typical electron-donor molecule.[38]

As shown in Figure 3, the average strength of donor−acceptor interactions of confined ice is not as strong as hexagonal ice and is rather close to that of liquid water, even though the structural and dynamical properties clearly suggest the phase behavior typical of a solid. When the temperature of confined water is decreased to 200 K in MD simulations, the donor−acceptor interactions vary only marginally (Figure S1). Water molecules in 1D ice experience a high degree of asymmetry in the strength of the first two strongest donor−


DOI: 10.1021/acs.jpclett.9b00921
J. Phys. Chem. Lett. 2019, 10, 2008−2016

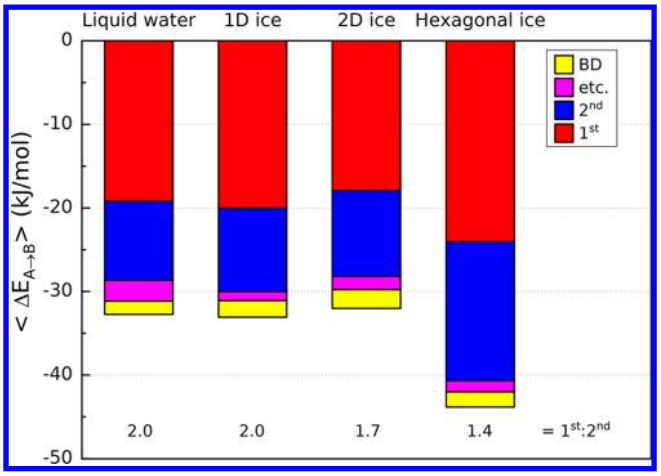


**Figure 3.** Average contributions to the total charge transfer energy from the occupied orbitals of electron-donor molecule A to the virtual orbitals of electron-acceptor molecule B for each system. Only the first two strongest interactions are shown while the rest are collected into the "etc." term. The "BD" term is the combined contribution of back-donation interactions.

acceptor interactions to the same extent as liquid water. A detailed analysis of this is presented in Figure S2.

To understand the origin of these unexpectedly different electronic signatures of low-dimensional ice and bulk ice, we analyzed the distribution of the intermolecular distance ($R_{O-O}$) and HB angle ($\beta$) (Figure 4) – the known dominant structural factors in determining the strength of donor–acceptor interactions in hydrogen bonding. Pentagonal 1D ice in CNT, referred to as ice nanotubes, typically forms two different types of HBs. The OH bonds pointing toward the axial and lateral direction of the CNT make inter- and intra-ring HBs respectively as shown in Figure 1a. We analyzed each HBs separately. Figure 4a shows that while the intra-ring HBs (red line) are arranged linearly ($\beta \sim 12°$), the inter-ring HBs (blue line) exhibit a wide range of angular distortions ($\beta \sim 20°$). The average oxygen–oxygen distance ($R_{O-O}$) of inter- and intra-ring HBs differ only by ~ 0.03 Å and are close to hexagonal ice. Thus, the high asymmetry in the strength of donor–acceptor interactions in 1D ice can be attributed to the difference in $\beta$ of inter and intra-ring HBs. The nature of the asymmetry in 1D ice is different from that in liquid water.[48,49]

In addition to the difference in the $R_{O-O}$ and $\beta$ distributions, we plotted the CT energy as a function of the HB angle ($\beta$) with the oxygen–oxygen distance ($R_{O-O}$) fixed at 2.8 Å (Figure 4, left panels) and vice versa as a function of the oxygen–oxygen distance ($R_{O-O}$) with the HB angle ($\beta$) fixed at 13° (Figure 4, right panels). First of all, the relationship between the CT energy and geometric parameters exhibits general trends common to all HBs. For example, the exponential decay of the CT energy with increase in the intermolecular distance ($R_{O-O}$) indicates that the CT term in all systems is a short-range attractive interaction originating from the orbital overlap. However, the comparison of the CT energy dependence on $R_{O-O}$ and $\beta$ is suggestive of the different structure the HB networks in confined and bulk systems. It is important to note that the distributions of the CT energy as a function of the $R_{O-O}$ and $\beta$ for confined and bulk ice do not overlap. For the 1D ice, the inter-ring CT energy is, on average, ~4 kJ/mol lower than the intra-ring CT energy at the same $R_{O-O}$ and $\beta$ while most intra-ring CT energy overlaps with hexagonal ice (Figure 4a). For the 2D ice, the average oxygen–oxygen distance ($R_{O-O}$) in our MD simulation, 2.82 ± 0.1 Å, is in good agreement with experiments (2.83 ± 0.03 Å).[22] Differences in the oxygen–oxygen distance ($R_{O-O}$) (by 0.04 Å) and in HB angle $\beta$ (by 3.2°) between 2D ice and hexagonal ice, however, are insufficient to explain the weaker CT interactions in 2D ice in Figure 3. Figure 4b shows that the 2D ice also exhibits lower CT energy by ~4 kJ/mol on average than hexagonal ice at the same $R_{O-O}$ and $\beta$ like inter- and intra-ring HBs in 1D ice. This unexpected result suggests the weaker CT interactions in confined ice cannot be explained solely by the difference in these two geometric parameters. Therefore, we sought the origin of the different electronic signatures among other structural features.

We considered geometric parameters that describe how the local molecular environment deviate from the ideal tetrahedral configuration. In bulk water, the four valence orbitals in a water molecule are $sp^3$-hybridized. Two of them are involved in covalent OH bonds, and the remaining two are associated with the lone electron pairs, forming a tetrahedral structure. Geometrically, the tetrahedral HB network found in hexagonal ice is not compatible with 2D planar channels. In other words, water molecules confined between two graphene layers 0.6 nm apart adopt the planar square-like bonding patterns (Figure 1b) instead of conventional tetrahedral configuration. This highly confined environment allows water molecules to be involved in 4-fold coordination in the lateral direction only to satisfy the ice rule with a double donor and a double acceptor except for defective lattice sites. The spatial orientation of oxygen atoms of the two electron-accepting neighbors can be characterized with the joint probability distributions $P(\theta,\varphi)$ revealing the structural difference of 2D and hexagonal ice. $\theta$ is defined as the angle between the interoxygen vector and the plane of the electron-donor molecule, whereas $\varphi$ is the angle between the interoxygen vector and the plane bisecting the HOH angle of the electron donor and normal to its molecular plane (Figure 5a). For hexagonal ice, $P(\theta,\varphi)$ exhibits a clear peak ($\theta$ = 51°, $\varphi$ = 0°) near the tetrahedral position as expected. On the other hand, what seems to be unique for the 2D ice is that all atoms in electron-accepting molecules are located in the nearly same plane parallel to the graphene. The peak of $P(\theta,\varphi)$ is located at near-zero $\theta$. Therefore, the position of electron-accepting neighbors is substantially deviated from the well-known lone pair sites of $sp^3$-hybridized O atom. We also found that $P(\theta,\varphi)$ of inter-ring HBs in 1D ice resembles that of 2D ice, whereas $P(\theta,\varphi)$ of intra-ring HBs resembles that of hexagonal ice. The 1D ice can be considered a mixture of two types of orientations (Figure 5e,f). Hence, the highly asymmetric electronic donor–acceptor interactions in 1D ice shown in Figure 3 originate from both the nontetrahedral orientation (Figure 5e) as well as the angular distortion of HBs (Figure 4a). This interpretation also is consistent with the vibrational spectroscopy data[58] that give rise to two different vibrational features: intra-ring HBs exhibit frequencies like those found in bulk water, whereas inter-ring HBs exhibit an unusual stretching frequency at 3507 $cm^{-1}$.

Although the absolute contribution of CT energy to total HB interaction energy is still a matter of debate depending on the method,[33,38,40,41,52−54] it is clear that the degree of covalent nature of HBs caused by CT becomes more pronounced in condensed phase when the intermolecular


DOI: 10.1021/acs.jpclett.9b00921
J. Phys. Chem. Lett. 2019, 10, 2008−2016

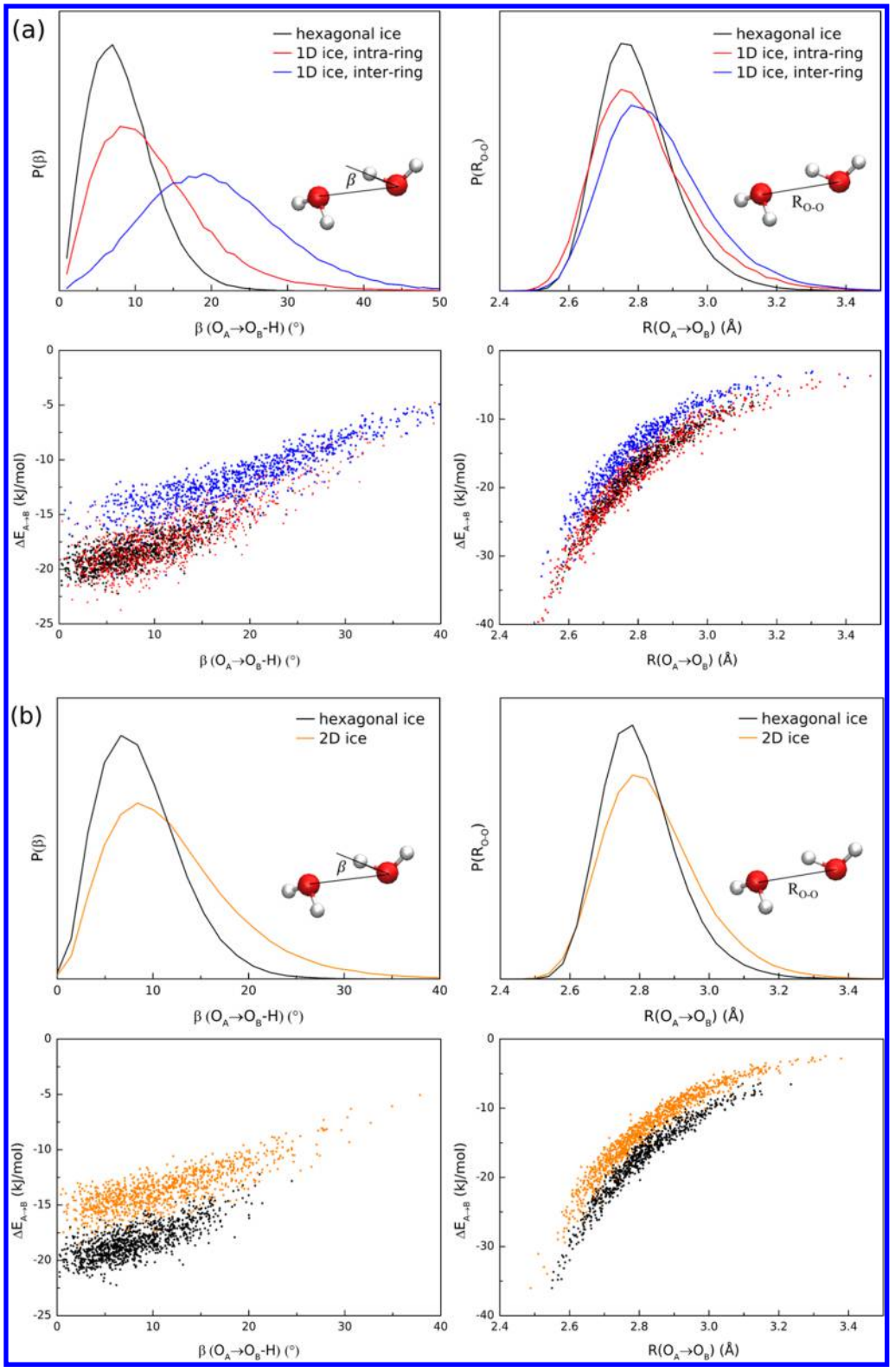


**Figure 4.** Distributions of the HB angle ($\beta$) and oxygen−oxygen distance ($R_{O-O}$) from classical MD simulations and dependence of the CT energy on these geometric parameters. The inset shows the definitions of $\beta$ and $R_{O-O}$. In the left panels, the CT energy is plotted as a function of the HB angle with the oxygen−oxygen distance ($R_{O-O}$) fixed at 2.8 Å. In the right panels, the CT energy is shown as a function of the oxygen−oxygen distance ($R_{O-O}$) with the HB angle fixed at 13°. (a) The intra-ring HB, inter-ring HB, and hexagonal ice are plotted as red, blue, and black, respectively. (b) The 2D ice is plotted as orange.

distance gets closer.[59−61] To estimate how the donor−acceptor interaction depends on the relative orientation of the hydrogen-bonded pair of water molecules, the CT energy is calculated as a function of two angular coordinates $\theta$ and $\varphi$ using the isolated water dimer with the intermolecular distance fixed to 2.82 Å. The resulting ALMO EDA contour



DOI: 10.1021/acs.jpclett.9b00921
J. Phys. Chem. Lett. 2019, 10, 2008−2016

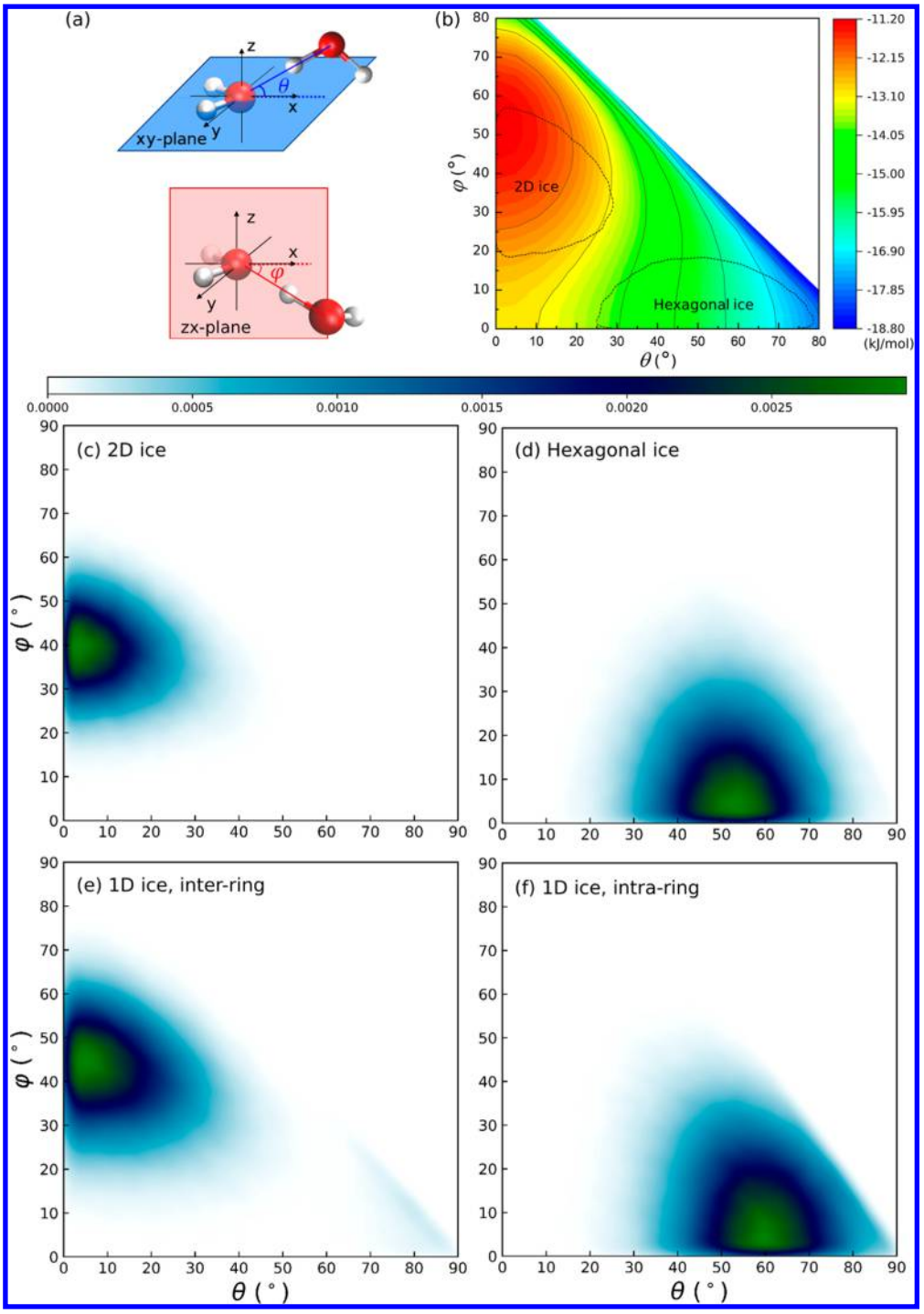


**Figure 5.** (a) Definitions of $\theta$ and $\varphi$. $\theta$ is defined as the angle between the interoxygen vector and the plane of the electron-donor molecule. The three atoms of the electron-donor molecule lie in the *xy*-plane. $\varphi$ is the angle between the interoxygen vector and the plane bisecting the HOH angle of the electron donor and normal to its molecular plane. (b) Contour plot of CT energy as a function of $\theta$ and $\varphi$ in a water dimer. The solid line represents the contour line of CT energy, and the dashed line represents the region where 2D ice and hexagonal ice have 90% probability distributions $P(\theta,\varphi)$ (see parts c and d). $R_{O-O}$ and $\beta$ shown in Figure 4 remained fixed during rotation of a molecule. $R_{O-O}$ is chosen as the averaged value of 2D ice (2.82 Å) and $\beta$ is set to zero. Detailed computational setup is the same as in this work. (c–f) Joint probability distributions $P(\theta,\varphi)$ of O atoms for the (c) 2D ice, (d) hexagonal ice and (e, f) 1D ice of inter- and intra-ring HB.

plot of a water dimer (Figure 5b) demonstrates clearly that the CT interaction is energetically less favorable when the dimer structure is constrained to resemble 2D ice structure from the conventional tetrahedral HB network of water, largely due to the different contribution of the p-like molecular orbital perpendicular to the molecular plane.[62,63] Quantitatively, the magnitude of CT energy of water dimer configurations typical of 2D ice is, on average, estimated to be ~4 kJ/mol lower than those typical of hexagonal ice by unfavorable relative orientation of molecules, and this difference is quite close to the CT energy difference (~4 kJ/mol) for the actual 2D and 3D condensed phases of ice for


DOI: 10.1021/acs.jpclett.9b00921
J. Phys. Chem. Lett. 2019, 10, 2008–2016

the same $R_{O-O}$ and $\beta$ due to confinement-induced constraints (Figure 4). Thus, the nontetrahedral orientation of 2D ice and half of 1D ice (inter-ring HB) additionally makes the strength of donor−acceptor interactions weaker and explains reduced CT energy at the same HB angle ($\beta$) and oxygen−oxygen distance ($R_{O-O}$) in Figure 4.

Our observation that donor−acceptor interactions are reduced in confined water has important implications for its modeling. Most empirical force fields used for water modeling do not include CT interactions explicitly. The absence of these interactions in the analytical force-field equation is instead compensated by the increased strength of the electrostatic and/or polarization interactions.[44] The compensating terms are traditionally tuned to reproduce properties of bulk water, not properties of low-dimensional confined water. While the structure of low-dimensional water obtained here with the SPC/E force field agrees well with the experimentally available data, comparative EDA demonstrates that, electronically, donor−acceptor interactions are different in bulk and confined ice and suggests that the missing CT interactions in confined water are improperly compensated in the commonly employed force fields. This implies that the properties sensitive to the strength of donor−acceptor interactions will be poorly described in simulations of low-dimensional water and that additional research efforts might be necessary to validate and perhaps optimize computational models to reproduce dynamical, electric, and thermodynamic properties of low-dimensional water reliably. We also note that the nuclear quantum effects of confined ice may be different from those in bulk hexagonal ice due to vastly different HB orientations, and estimating the influence of such effects on various properties of confined water would thus be an interesting question to address in future studies.

In summary, we utilized energy decomposition method based on ALMOs to analyze the strength of donor−acceptor orbital interactions in ice confined in low dimensions. Our MD simulations show that ice in (8, 8) CNT and between two graphene layers form well-aligned structures and exhibit phase behavior typical of a solid. However, the strength and patterns of quantum mechanical donor−acceptor interactions are confined ice is demonstrated to resemble that of bulk liquid water instead of bulk ice. A careful geometric analysis demonstrates the origins of this interesting phenomenon. In planar 2D ice, electron-transfer effects are reduced because of its highly nontetrahedral structure. On the other hand, molecules in 1D ice exhibit weaker electron-donation interactions and high degree of asymmetry due to both the nontetrahedral orientation and the angular distortion in the inter-ring HBs.

## COMPUTATIONAL METHODS

*Classical Molecular Dynamics Simulation.* We performed classical MD simulations of water with the extended simple point charge (SPC/E)[57] water model using the LAMMPS package.[64] The MD simulations were carried out in the constant volume and temperature (*NVT*) ensemble at 300 K with periodic boundary condition for confined water. Initial configurations for 1D system were taken from Pascal et al.[65] To determine the initial structures of 2D system, we performed MD simulations as illustrated in Figure S3. We found that "square ice" is formed between graphene layers under ambient conditions (1 atm, 300 K) using the water−carbon interactions parameters taken from Pascal et al.[65] We note that the previous *ab initio*[29−31] and force field[18,22−24,27,28] investigations also predicted the formation of square ice under different (e.g., high pressure) conditions, but the structure of the resulting square ice was similar to the present configurations. SHAKE algorithm is used to constrain the bond lengths and angle in water molecules with tolerance of $10^{-4}$. The positions of carbon atoms are fixed during the MD simulations because the flexibility of the confining surface in this configuration is insensitive to results.[22,27] We used a time step of 1.0 fs, the particle−particle particle−mesh (PPPM) method for long-range coulomb interactions with a cutoff of 12 Å and the inner and outer cutoff distance of was 10 and 12 Å for Lennard-Jones interactions. From each 10 ns run, we used the last 5 ns of trajectories for analysis. For comparison, we also performed MD simulation of bulk, liquid water with density of 0.996 g/cm$^3$ at 300 K and hexagonal ice with density of 0.926 g/cm$^3$ at 200 K using the same computational setup.

*Energy-Decomposition Analysis.* ALMO EDA for periodic systems was performed using the CP2K package for 1001 equidistant snapshots separated by 5 ps from the 5 ns trajectory for each system. CP2K employed the mixed Gaussian and plane wave approach, which is ideal for ALMO EDA because the localized atom-centered Gaussian basis sets are required for the construction of absolutely localized molecular orbitals, while plane waves are used to represent the charge density for computational efficiency. Molecular orbitals in all ALMO EDA calculations were represented by a triple-$\zeta$ Gaussian basis set with two sets of polarization functions[66] (TZV2P). A high-energy cutoff of 500 Ry was used to describe the electron density. The exchange correlation energy was approximated with the BLYP functional[67,68] with D3 dispersion correction of Grimme.[69−71] The Brillouin zone was sampled at the Γ-point and separable norm-conserving pseudopotentials were used to describe the interactions between the valence electrons and the ionic cores.[72] We remove carbon atoms from all trajectories to focus on the interaction between water molecules because the water−wall interaction in hydrophobic confinements is much weaker than the interaction between water molecules, and this does not affect EDA.

## ASSOCIATED CONTENT

### Supporting Information

The Supporting Information is available free of charge on the ACS Publications website at DOI: 10.1021/acs.jpclett.9b00921.

Donor−acceptor interactions of 1D and 2D ice at 200 K, asymmetry of donor−acceptor interactions in the 1D ice, and the density of 2D ice in MD simulations (PDF)

## AUTHOR INFORMATION


### Corresponding Authors

*(R.Z.K.) E-mail: rustam.khaliullin@mcgill.ca.
*(Y.J.) E-mail: ysjn@kaist.ac.kr.

### ORCID

Rustam Z. Khaliullin: 0000-0002-9073-6753
Yousung Jung: 0000-0003-2615-8394


### Notes

The authors declare no competing financial interest.



DOI: 10.1021/acs.jpclett.9b00921
J. Phys. Chem. Lett. 2019, 10, 2008−2016

## ■ ACKNOWLEDGMENTS

The financial support for his research is provided by the Korean Government through the National Research Foundation of Korea (NRF-2016K1A3A1A12953725) with further support coming from the Climate Change Research Hub of KAIST (Grant No. N01150139). The research is partially funded by Compute Canada and the Natural Sciences and Engineering Research Council of Canada through a Discovery Grant (RGPIN-2016-05059).

## ■ REFERENCES

(1) Ghosh, S.; Sood, A. K.; Kumar, N. Carbon Nanotube Flow Sensors. *Science* **2003**, *299*, 1042−1044.
(2) Kalra, A.; Garde, S.; Hummer, G. Osmotic Water Transport through Carbon Nanotube Membranes. *Proc. Natl. Acad. Sci. U. S. A.* **2003**, *100*, 10175−10180.
(3) Dillon, A. C. Carbon Nanotubes for Photoconversion and Electrical Energy Storage. *Chem. Rev.* **2010**, *110*, 6856−6872.
(4) Nair, R. R.; Wu, H. A.; Jayaram, P. N.; Grigorieva, I. V.; Geim, A. K. Unimpeded Permeation of Water through Helium-Leak-Tight Graphene-Based Membranes. *Science* **2012**, *335*, 442−444.
(5) Park, H. G.; Jung, Y. Carbon Nanofluidics of Rapid Water Transport for Energy Applications. *Chem. Soc. Rev.* **2014**, *43*, 565−576.
(6) Gallo, P.; Rovere, M.; Chen, S. H. Dynamic Crossover in Supercooled Confined Water: Understanding Bulk Properties through Confinement. *J. Phys. Chem. Lett.* **2010**, *1*, 729−733.
(7) Koga, K.; Tanaka, H.; Zeng, X. C. First-Order Transition in Confined Water between High-Density Liquid and Low-Density Amorphous Phases. *Nature* **2000**, *408*, 564−567.
(8) Koga, K.; Gao, G. T.; Tanaka, H.; Zeng, X. C. Formation of Ordered Ice Nanotubes inside Carbon Nanotubes. *Nature* **2001**, *412*, 802−805.
(9) Bai, J.; Su, C. R.; Parra, R. D.; Zeng, X. C.; Tanaka, H.; Koga, K.; Li, J. M. Ab Initio Studies of Quasi-One-Dimensional Pentagon and Hexagon Ice Nanotubes. *J. Chem. Phys.* **2003**, *118*, 3913−3916.
(10) Mashl, R. J.; Joseph, S.; Aluru, N. R.; Jakobsson, E. Anomalously Immobilized Water: A New Water Phase Induced by Confinement in Nanotubes. *Nano Lett.* **2003**, *3*, 589−592.
(11) Koga, K.; Tanaka, H. Phase Diagram of Water between Hydrophobic Surfaces. *J. Chem. Phys.* **2005**, *122*, 104711.
(12) Majumder, M.; Chopra, N.; Andrews, R.; Hinds, B. J. Nanoscale Hydrodynamics: Enhanced Flow in Carbon Nanotubes. *Nature* **2005**, *438*, 44.
(13) Holt, J. K.; Park, H. G.; Wang, Y.; Stadermann, M.; Artyukhin, A. B.; Grigoropoulos, C. P.; Noy, A.; Bakajin, O. Fast Mass Transport through Sub-2-Nanometer Carbon Nanotubes. *Science* **2006**, *312*, 1034−1037.
(14) Takaiwa, D.; Hatano, I.; Koga, K.; Tanaka, H. Phase Diagram of Water in Carbon Nanotubes. *Proc. Natl. Acad. Sci. U. S. A.* **2008**, *105*, 39−43.
(15) Kumar, P.; Buldyrev, S. V.; Starr, F. W.; Giovambattista, N.; Stanley, H. E. Thermodynamics, Structure, and Dynamics of Water Confined between Hydrophobic Plates. *Phys. Rev. E* **2005**, *72*, No. 051503.
(16) Giovambattista, N.; Rossky, P. J.; Debenedetti, P. G. Phase Transitions Induced by Nanoconfinement in Liquid Water. *Phys. Rev. Lett.* **2009**, *102*, No. 050603.
(17) Han, S. H.; Choi, M. Y.; Kumar, P.; Stanley, H. E. Phase Transitions in Confined Water Nanofilms. *Nat. Phys.* **2010**, *6*, 685−689.
(18) Jiao, S.; Duan, C.; Xu, Z. Structures and Thermodynamics of Water Encapsulated by Graphene. *Sci. Rep.* **2017**, *7*, 2646.
(19) Zangi, R.; Mark, A. E. Monolayer Ice. *Phys. Rev. Lett.* **2003**, *91*, No. 025502.
(20) Zhao, W. H.; Bai, J.; Yuan, L. F.; Yang, J. L.; Zeng, X. C. Ferroelectric Hexagonal and Rhombic Monolayer Ice Phases. *Chem. Sci.* **2014**, *5*, 1757−1764.
(21) Zhao, W. H.; Wang, L.; Bai, J.; Yuan, L. F.; Yang, J.; Zeng, X. C. Highly Confined Water: Two-Dimensional Ice, Amorphous Ice, and Clathrate Hydrates. *Acc. Chem. Res.* **2014**, *47*, 2505−2513.
(22) Algara-Siller, G.; Lehtinen, O.; Wang, F. C.; Nair, R. R.; Kaiser, U.; Wu, H. A.; Geim, A. K.; Grigorieva, I. V. Square Ice in Graphene Nanocapillaries. *Nature* **2015**, *519*, 443−445.
(23) Gao, Z.; Giovambattista, N.; Sahin, O. Phase Diagram of Water Confined by Graphene. *Sci. Rep.* **2018**, *8*, 6228.
(24) Raju, M.; van Duin, A.; Ihme, M. Phase Transitions of Ordered Ice in Graphene Nanocapillaries and Carbon Nanotubes. *Sci. Rep.* **2018**, *8*, 3851.
(25) Agrawal, K. V.; Shimizu, S.; Drahushuk, L. W.; Kilcoyne, D.; Strano, M. S. Observation of Extreme Phase Transition Temperatures of Water Confined inside Isolated Carbon Nanotubes. *Nat. Nanotechnol.* **2017**, *12*, 267−273.
(26) Zhou, W.; Yin, K.; Wang, C.; Zhang, Y.; Xu, T.; Borisevich, A.; Sun, L.; Idrobo, J. C.; Chisholm, M. F.; Pantelides, S. T.; et al. The Observation of Square Ice in Graphene Questioned. *Nature* **2015**, *528*, E1−E2.
(27) Ruiz Pestana, L.; Felberg, L. E.; Head-Gordon, T. Coexistence of Multilayered Phases of Confined Water: The Importance of Flexible Confining Surfaces. *ACS Nano* **2018**, *12*, 448−454.
(28) Zhu, Y.; Wang, F.; Bai, J.; Zeng, X. C.; Wu, H. Compression Limit of Two-Dimensional Water Constrained in Graphene Nanocapillaries. *ACS Nano* **2015**, *9*, 12197−12204.
(29) Corsetti, F.; Matthews, P.; Artacho, E. Structural and Configurational Properties of Nanoconfined Monolayer Ice from First Principles. *Sci. Rep.* **2016**, *6*, 18651.
(30) Chen, J.; Schusteritsch, G.; Pickard, C. J.; Salzmann, C. G.; Michaelides, A. Two Dimensional Ice from First Principles: Structures and Phase Transitions. *Phys. Rev. Lett.* **2016**, *116*, No. 025501.
(31) Chen, J.; Zen, A.; Brandenburg, J. G.; Alfe, D.; Michaelides, A. Evidence for Stable Square Ice from Quantum Monte Carlo. *Phys. Rev. B: Condens. Matter Mater. Phys.* **2016**, *94*, 220102.
(32) Stevens, W. J.; Fink, W. H. Frozen Fragment Reduced Variational Space Analysis of Hydrogen-Bonding Interactions: Application to the Water Dimer. *Chem. Phys. Lett.* **1987**, *139*, 15−22.
(33) Glendening, E. D.; Streitwieser, A. Natural Energy Decomposition Analysis: An Energy Partitioning Procedure for Molecular-Interactions with Application to Weak Hydrogen-Bonding, Strong Ionic, and Moderate Donor-Acceptor Interactions. *J. Chem. Phys.* **1994**, *100*, 2900−2909.
(34) Chen, W.; Gordon, M. S. Energy Decomposition Analyses for Many-Body Interaction and Applications to Water Complexes. *J. Phys. Chem.* **1996**, *100*, 14316−14328.
(35) Mo, Y. R.; Gao, J. L.; Peyerimhoff, S. D. Energy Decomposition Analysis of Intermolecular Interactions Using a Block-Localized Wave Function Approach. *J. Chem. Phys.* **2000**, *112*, 5530−5538.
(36) Glendening, E. D. Natural Energy Decomposition Analysis: Extension to Density Functional Methods and Analysis of Cooperative Effects in Water Clusters. *J. Phys. Chem. A* **2005**, *109*, 11936−11940.
(37) Piquemal, J. P.; Marquez, A.; Parisel, O.; Giessner-Prettre, C. A CSOV Study of the Difference between HF and DFT Intermolecular Interaction Energy Values: The Importance of the Charge Transfer Contribution. *J. Comput. Chem.* **2005**, *26*, 1052−1062.
(38) Khaliullin, R. Z.; Cobar, E. A.; Lochan, R. C.; Bell, A. T.; Head-Gordon, M. Unravelling the Origin of Intermolecular Interactions Using Absolutely Localized Molecular Orbitals. *J. Phys. Chem. A* **2007**, *111*, 8753−8765.
(39) Cobar, E. A.; Horn, P. R.; Bergman, R. G.; Head-Gordon, M. Examination of the Hydrogen-Bonding Networks in Small Water Clusters (N = 2−5, 13, 17) Using Absolutely Localized Molecular


DOI: 10.1021/acs.jpclett.9b00921
*J. Phys. Chem. Lett.* 2019, 10, 2008−2016

Orbital Energy Decomposition Analysis. *Phys. Chem. Chem. Phys.* **2012**, *14*, 15328−15339.
(40) Szalewicz, K. Symmetry-Adapted Perturbation Theory of Intermolecular Forces. *WIREs Comput. Mol. Sci.* **2012**, *2*, 254−272.
(41) Misquitta, A. J. Charge Transfer from Regularized Symmetry-Adapted Perturbation Theory. *J. Chem. Theory Comput.* **2013**, *9*, 5313−5326.
(42) Wang, B.; Jiang, W.; Dai, X.; Gao, Y.; Wang, Z.; Zhang, R. Q. Molecular Orbital Analysis of the Hydrogen Bonded Water Dimer. *Sci. Rep.* **2016**, *6*, 22099.
(43) Stone, A. J. Natural Bond Orbitals and the Nature of the Hydrogen Bond. *J. Phys. Chem. A* **2017**, *121*, 1531−1534.
(44) Shi, Y.; Scheiber, H.; Khaliullin, R. Z. Contribution of the Covalent Component of the Hydrogen-Bond Network to the Properties of Liquid Water. *J. Phys. Chem. A* **2018**, *122*, 7482−7490.
(45) Lenz, A.; Ojamäe, L. Theoretical IR Spectra for Water Clusters $(H_2O)_n$ ($n$ = 6−22, 28, 30) and Identification of Spectral Contributions from Different H-Bond Conformations in Gaseous and Liquid Water. *J. Phys. Chem. A* **2006**, *110*, 13388−13393.
(46) Ramos-Cordoba, E.; Lambrecht, D. S.; Head-Gordon, M. Charge-Transfer and the Hydrogen Bond: Spectroscopic and Structural Implications from Electronic Structure Calculations. *Faraday Discuss.* **2011**, *150*, 345−362. See also: RSC. General discussion. *Faraday Discuss.* **2011**, *150*, 391−418.
(47) Zhang, C.; Khaliullin, R. Z.; Bovi, D.; Guidoni, L.; Kuhne, T. D. Vibrational Signature of Water Molecules in Asymmetric Hydrogen Bonding Environments. *J. Phys. Chem. Lett.* **2013**, *4*, 3245−3250.
(48) Kuhne, T. D.; Khaliullin, R. Z. Electronic Signature of the Instantaneous Asymmetry in the First Coordination Shell of Liquid Water. *Nat. Commun.* **2013**, *4*, 1450.
(49) Kuhne, T. D.; Khaliullin, R. Z. Nature of the Asymmetry in the Hydrogen-Bond Networks of Hexagonal Ice and Liquid Water. *J. Am. Chem. Soc.* **2014**, *136*, 3395−3399.
(50) Elgabarty, H.; Khaliullin, R. Z.; Kuhne, T. D. Covalency of Hydrogen Bonds in Liquid Water Can Be Probed by Proton Nuclear Magnetic Resonance Experiments. *Nat. Commun.* **2015**, *6*, 8318.
(51) Fransson, T.; Harada, Y.; Kosugi, N.; Besley, N. A.; Winter, B.; Rehr, J. J.; Pettersson, L. G.; Nilsson, A. X-Ray and Electron Spectroscopy of Water. *Chem. Rev.* **2016**, *116*, 7551−7569.
(52) Weinhold, F. Natural Bond Orbital Methods. In *Encyclopedia of Computational Chemistry*; Wiley: 2002.
(53) Kitaura, K.; Morokuma, K. A New Energy Decomposition Scheme for Molecular Interactions within the Hartree-Fock Approximation. *Int. J. Quantum Chem.* **1976**, *10*, 325−340.
(54) Bagus, P. S.; Hermann, K.; Bauschlicher, C. W. A New Analysis of Charge-Transfer and Polarization for Ligand-Metal Bonding: Model Studies of $Al_4co$ and $Al_4NH_3$. *J. Chem. Phys.* **1984**, *80*, 4378−4386.
(55) Horn, P. R.; Head-Gordon, M. Polarization Contributions to Intermolecular Interactions Revisited with Fragment Electric-Field Response Functions. *J. Chem. Phys.* **2015**, *143*, 114111.
(56) Khaliullin, R. Z.; Kuhne, T. D. Microscopic Properties of Liquid Water from Combined Ab Initio Molecular Dynamics and Energy Decomposition Studies. *Phys. Chem. Chem. Phys.* **2013**, *15*, 15746−15766.
(57) Berendsen, H. J. C.; Grigera, J. R.; Straatsma, T. P. The Missing Term in Effective Pair Potentials. *J. Phys. Chem.* **1987**, *91*, 6269−6271.
(58) Byl, O.; Liu, J. C.; Wang, Y.; Yim, W. L.; Johnson, J. K.; Yates, J. T., Jr. Unusual Hydrogen Bonding in Water-Filled Carbon Nanotubes. *J. Am. Chem. Soc.* **2006**, *128*, 12090−12097.
(59) Desiraju, G. R. Hydrogen Bridges in Crystal Engineering: Interactions without Borders. *Acc. Chem. Res.* **2002**, *35*, 565−573.
(60) Grabowski, S. J.; Sokalski, W. A.; Dyguda, E.; Leszczynski, J. Quantitative Classification of Covalent and Noncovalent H-Bonds. *J. Phys. Chem. B* **2006**, *110*, 6444−6446.
(61) Grabowski, S. J. What Is the Covalency of Hydrogen Bonding? *Chem. Rev.* **2011**, *111*, 2597−625.
(62) Khaliullin, R. Z.; Bell, A. T.; Head-Gordon, M. Electron Donation in the Water-Water Hydrogen Bond. *Chem. - Eur. J.* **2009**, *15*, 851−855.
(63) Brini, E.; Fennell, C. J.; Fernandez-Serra, M.; Hribar-Lee, B.; Luksic, M.; Dill, K. A. How Water's Properties Are Encoded in Its Molecular Structure and Energies. *Chem. Rev.* **2017**, *117*, 12385−12414.
(64) Plimpton, S. Fast Parallel Algorithms for Short-Range Molecular-Dynamics. *J. Comput. Phys.* **1995**, *117*, 1−19.
(65) Pascal, T. A.; Goddard, W. A.; Jung, Y. Entropy and the Driving Force for the Filling of Carbon Nanotubes with Water. *Proc. Natl. Acad. Sci. U. S. A.* **2011**, *108*, 11794−11798.
(66) VandeVondele, J.; Hutter, J. Gaussian Basis Sets for Accurate Calculations on Molecular Systems in Gas and Condensed Phases. *J. Chem. Phys.* **2007**, *127*, 114105.
(67) Becke, A. D. Density-Functional Exchange-Energy Approximation with Correct Asymptotic Behavior. *Phys. Rev. A: At., Mol., Opt. Phys.* **1988**, *38*, 3098−3100.
(68) Lee, C. T.; Yang, W. T.; Parr, R. G. Development of the Colle-Salvetti Correlation-Energy Formula into a Functional of the Electron Density. *Phys. Rev. B: Condens. Matter Mater. Phys.* **1988**, *37*, 785−789.
(69) Grimme, S. Accurate Description of Van Der Waals Complexes by Density Functional Theory Including Empirical Corrections. *J. Comput. Chem.* **2004**, *25*, 1463−1473.
(70) Grimme, S. Semiempirical GGA-Type Density Functional Constructed with a Long-Range Dispersion Correction. *J. Comput. Chem.* **2006**, *27*, 1787−1799.
(71) Grimme, S.; Antony, J.; Ehrlich, S.; Krieg, H. A Consistent and Accurate Ab Initio Parametrization of Density Functional Dispersion Correction (DFT-D) for the 94 Elements H-Pu. *J. Chem. Phys.* **2010**, *132*, 154104.
(72) Hartwigsen, C.; Goedecker, S.; Hutter, J. Relativistic Separable Dual-Space Gaussian Pseudopotentials from H to Rn. *Phys. Rev. B: Condens. Matter Mater. Phys.* **1998**, *58*, 3641−3662.


DOI: 10.1021/acs.jpclett.9b00921
*J. Phys. Chem. Lett.* 2019, 10, 2008−2016